

Fracture Behavior of 6061 Al-Alloy Pipes under Bursting Loads with Crack Depth Variation

D.U.M. Manikanta, A.Chennakesava Reddy

Abstract— In this paper 3D finite element analyses were performed to obtain fracture behavior of 6061 Al-alloy pipes subjected to internal bursting pressure. It was observed that the large deformations have promoted the path dependence of the J-integral. It was noticed that the J-integral was dependent on the deformation and the crack area. The values of KII and KIII stress intensity factors along the crack-front were very small and, the, mode-I was the dominant fracture mode.

Index Terms— 6061, bursting pressure, fracture, crack depth, pipes, J-integral, stress intensity factors.

1 INTRODUCTION

PIPELINES are being used for the transport of gas and oil. The most important parameters in designing pipelines are the pressure and temperature of the conveying media. Other parameters such as properties of the fluid, the elevation and slope of the terrain, and dynamic effects such as live and dead loads, earthquakes, waves and thermal expansion and contraction, should also be considered. The major concern of pipes is to maintain its geometric integrity to ensure they are safe and effective during operation to avoid unforeseen disaster. One of the major geometric integrity of the pipe is cracks on its surface. The wall thinning on a pipe due to corrosion, results in localized pit with different depths and lengths on its internal and external surfaces [1], [2]. The codes such as BS 7910 [3] and DNV RP-F101 [4] are the semi-empirical methods used for the assessment of the integrity of pipes. The operating pressure calculation and consequent wall thickness of gas transmission pipelines can be obtained from ASME B31.8 (ASMEB31.8 2012):

$$P = (2 \sigma t) / D \times F \times E \times T \quad (1)$$

where P is the design pressure (Mpa), σ is the specified minimum yield strength (MPa), t is the nominal wall thickness (mm), D is the nominal outside diameter (mm), F is the design factor, E is the longitudinal joint factor and T is the temperature derating factor.

As demonstrated in figure 1, analysis of fracture mechanics is described as three pure modes. In mode one (I) or "opening mode" the displacement of crack surfaces due to normal stresses, are perpendicular to the plane of the crack. In forward shear or mode two (II) or "sliding mode", the displacement of crack surfaces is in the plane of the crack and normal to the crack front line. The "tearing mode" or mode three (III) is caused by anti plane shear and the crack surface displacements are parallel to the crack front line and in the plane of the crack. The SIF represented by capital K. The K subscripts I, II and III stands for different loading conditions.

In a pure elastic crack, stress singularity at the crack tip is dominant. Due to the yield stress of materials especially in metals, for stresses above the σ_y the material deforms plastically. So stress singularity cannot exist. Figure 2 illustrates an approximate stress distribution at the crack tip with a plastic zone. Irwin argues that the crack tip plasticity causes lower stiffness and larger displacements than in the elastic case [5].

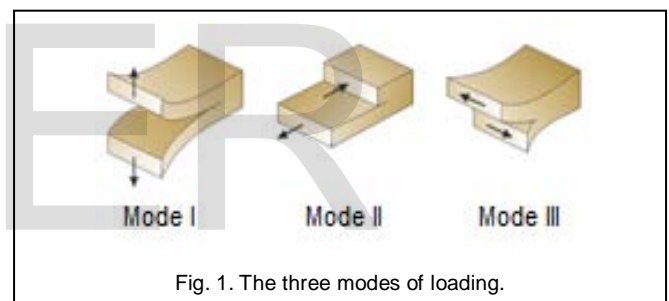


Fig. 1. The three modes of loading.

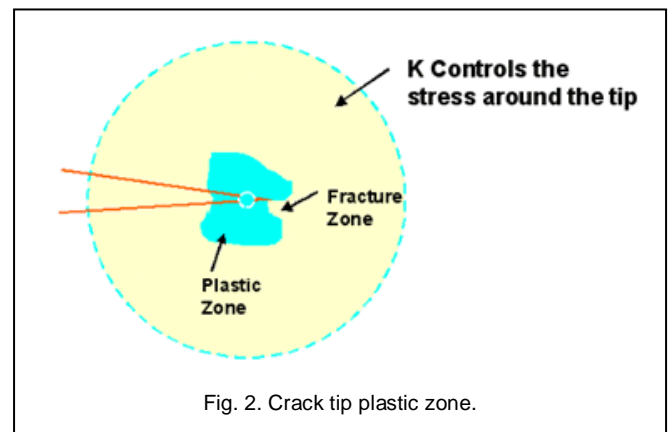


Fig. 2. Crack tip plastic zone.

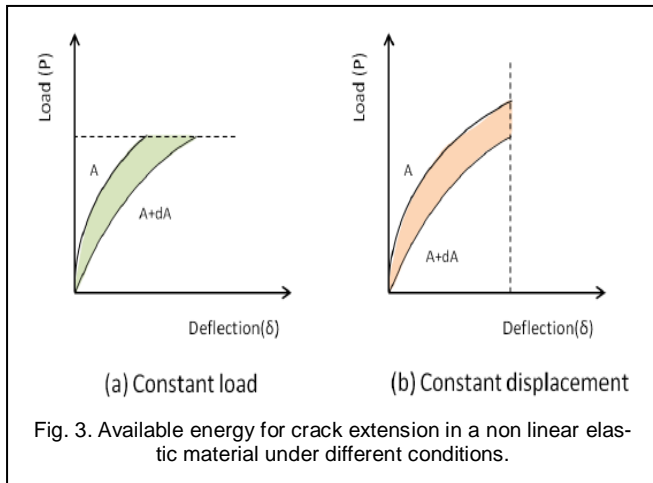
Similar to linear elastic cases, an energy release rate for nonlinear elastic bodies can be defined as the area on the load displacement diagram between crack areas A and A+dA, as shown in figure 3. The nonlinear energy release rate J, for constant load and constant displacement has been defined as:

$$J = \left| \frac{\partial \Pi}{\partial A} \right| \quad (2)$$

- D.U.M. Manikanta is currently pursuing masters degree program in advanced manufacturing systems, JNT University, Hyderabad, India, PH-+919491191783. E-mail: manikantademudu@gmail.com
- A. Chennakesava Reddy, Professor, JNT University, Hyderabad, India

Testing Conditions of Pipes

Test coupon	Diameter of pipe, D (mm)	Thickness of pipe, t (mm)	Length of pipe, L (mm)	Crack length, h (2a)	Crack width, w (mm)	Crack depth, d (mm)	Pressure, MPa
1	41.28	0.89	914	33.08	0.2	0.56	6.1
2	41.28	0.89	610	33.08	0.2	0.56	4.0
3	41.28	0.89	610	33.08	0.2	0.48	5.4
4	41.28	0.89	610	33.08	0.2	0.48	4.4
5	41.28	0.89	610	33.08	0.2	0.64	4.0
6	41.28	0.89	610	33.08	0.2	0.64	6.1
7	41.28	1.24	610	33.08	0.2	0.71	4.9
8	41.28	1.24	610	33.08	0.2	0.71	6.1
9	41.28	1.47	610	33.08	0.2	1.19	4.4
10	41.28	1.47	610	33.08	0.2	1.19	6.1



The finite element analysis (FEA) is one of the most efficient tools to quantify reliably the remaining strength of corroded pipes. Elastic-Plastic finite element models have been used to provide more accurate results in evaluating the corrosion defects [6]. ANSYS [7] can be used to numerically evaluate the collapse pressure of crack defects. When a corrosion/ flaw defect occurs on the internal or external pipe surface, the integrity of the pipe is reduced. The important parameters that determine the strength of a pipe are as follows [8]:

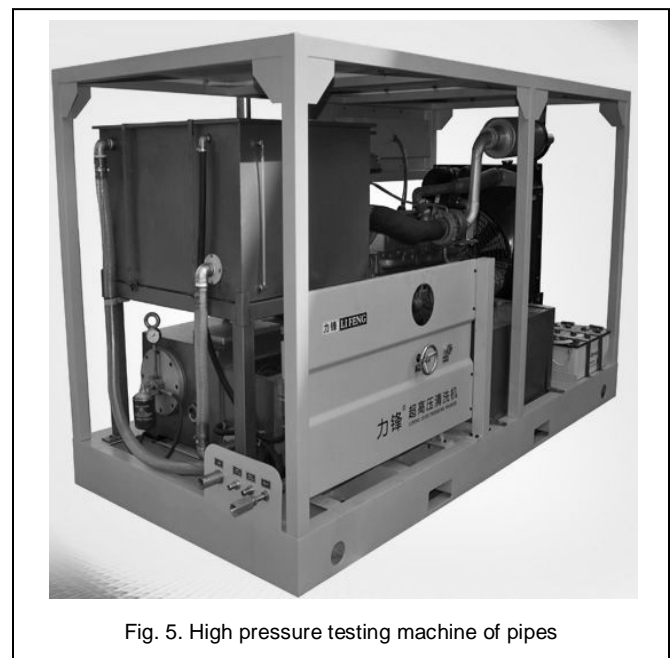
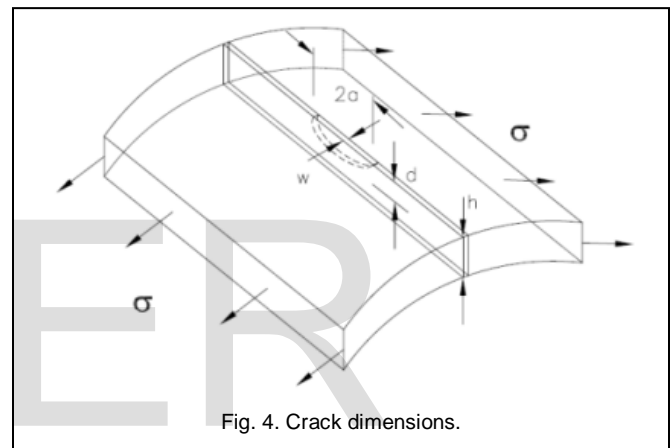
- Internal pressure
- Pipe Diameter
- Crack depth related to the wall thickness
- Crack length related to the pipe length
- Stress distribution
- Total deformation
- J-integral
- Stress intensity factors (SIFs): KI, KII and KIII

The present work is aimed at to study the finite element analysis of crack propagation and pipe bursting with predefined flaws of varying length and depth. The pipes are analyzed for various bursting pressures. As illustrated in figure 1, the longitudinal crack length is shown at 2a and the pipe is under an internal pressure loading of p, with the pipe thickness depicted as t.

2 MATERIALS AND METHODS

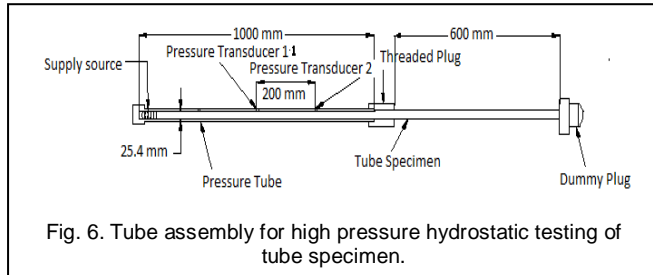
Experiments were performed on 6061 Al alloy pipes. Five types of 6061 Al-alloy tubes of different crack depths viz., 0.48 mm, 0.56 mm, 0.64 mm, 0.71 and 1.19 mm tubes of the same outer diameter (41.28 mm) were used for experimentation (table-1). A surface notch as shown in figure 4 made on the outer surface of the specimen was used as a preflaw for experimentation. Outer surface notches provide an indication of system response to discontinuities originating from the outer surface. The dimensions of notches are given in table 1. Outer surface notches were produced in the middle of the tube length by electric discharge machining (EDM). The specimens were coded as shown in table 1 for easy monitoring during experimentation.

TABLE 1



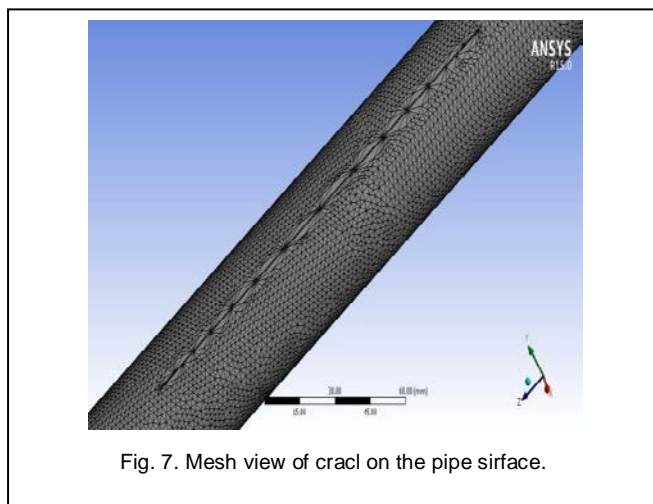
High pressure testing machine (2000 bar) as shown in figure 5 was used for hydrostatically testing of 6061 Al-alloy pipes. The tube specimen was fixed to the main pressure hose

of the testing unit with a threaded plug as shown in figure 6. On running motor of the pump the pressure was gradually developed, on increasing the pressure further gradually, the specimen was started yielding at the notch. When the pressure was still increased the specimen was burst at the notch. The specimen code and the corresponding pressure were recorded for each specimen.



3 FINITE ELEMENT MODELING

The cross-section of the pipe was crated in 2-D anf then it was extruded for the given pipe length along the z-direction [9]. The ANSYS code was used to model the pipe and initial semi-elliptical crack. The pipe was modeled with tetrahedron elements. The crack and pipe dimensions are given in table-1. The crack geometry is shown in figure 4. Fracture module method for crack generation required that elements be of higher order. Therefore, out of choice of tetrahedral elements of type SOLID 186 were chosen for accurate results [10], [11], [12]. Fine mesh was used to model the crack region. A three-dimensional semi-elliptical crack was initiated on the shaft surface. The crack was oriented with respect to pipe axis. In order to create the semi-elliptical crack onto to the surface, a local coordinate system was established. With reference to the local co-ordinate system and the crack was created on the outer surface of the pipe as shown in figure 7. The pressure was applied on the inner surface of pipe.



Stress intensity is defined as the largest of the absolute values of $\sigma_1 - \sigma_2$, $\sigma_2 - \sigma_3$, or $\sigma_3 - \sigma_1$ [13]:

$$\sigma_I = \text{MAX} (|\sigma_1 - \sigma_2|, |\sigma_2 - \sigma_3|, |\sigma_3 - \sigma_1|) \quad (3)$$

Stress intensity is related to the maximum shear stress:

$$\sigma_I = 2\tau_{\text{max}} \quad (4)$$

Elastic strain intensity is defined as the largest of the absolute values of $\epsilon_1 - \epsilon_2$, $\epsilon_2 - \epsilon_3$, or $\epsilon_3 - \epsilon_1$:

$$\epsilon_I = \text{MAX} (|\epsilon_1 - \epsilon_2|, |\epsilon_2 - \epsilon_3|, |\epsilon_3 - \epsilon_1|) \quad (5)$$

Elastic strain intensity is equal to the maximum shear elastic strain:

$$\epsilon_I = \gamma_{\text{max}} \quad (6)$$

The maximum equivalent stress safety tool is based on the maximum equivalent stress failure theory for ductile materials, also referred to as the von Mises-Hencky theory. The discretized form of the J-Integral is given by:

$$J = \sum_{ie=1}^{ne} \left[\sigma_{ij} \frac{\partial u_j}{\partial x_i} - w \delta_{ij} \right] \frac{\partial q}{\partial x_i} w_{iw} A_{ie} \quad (7)$$

where ne is the number of elements to be integrated, w_{iw} is the weight function, and A_{ie} is the area of the element represented by ie .

For higher-order elements (such as SOLID186), the q vector at midside nodes takes the averaged values from the corresponding corner nodes. For a 3-D problem, domain integral representation of the J-Integral becomes a volume integration, which again is evaluated over a group of elements. The implementation becomes more complicated; however, the principal is similar to the 2-D problem. The near-crack-tip behavior of stress is usually thought to be that of plane strain. K_I , K_{II} , K_{III} were obtained from KCALC command.

4 RESULTS AND DISCUSSION

The results from rhe finite element software ANSYS were verified with a few critical results through experimentation.

TABLE 2
 Deformation Results of Pipes

Test coupon	Total deformation, mm x e-02	Directional (along pipe depth) deformation, mm x e-02
1	7.5278	1.6371
2	6.0265	4.5013
3	6.6380	5.8265
4	4.4892	3.3092
5	6.2743	4.4518
6	9.7000	6.9910
7	4.6957	3.8338
8	5.7492	3.2556
9	5.7242	4.0913
10	7.0283	4.1647

4.1 Static Deformations

Table 2 gives the total deformation values of tested pipes with different crack geometry and bursting pressure. The effect of pipe thickness/crack depth (t/d) ($=0.89/0.64$) ratio on the total and directional deformations is plotted in figure 8. The t/d

ratio of 1.40 for test coupon 6 gave the maximum total and directional deformations of 0.0970 mm and 0.0699 mm respectively along the crack depth direction. The t/d ratio of 1.85 for test coupon 4 gave the minimum total and directional deformations of 0.0449 mm and 0.0331 mm respectively along the crack depth direction. In both the cases the bursting pressure was 6.1 MPa. The experimental fracture are compared with fracture results obtained from FEA for the test coupons 6 and 4 in figure 9 and 10 respectively. The FEA results were in good agreement with experimental values.

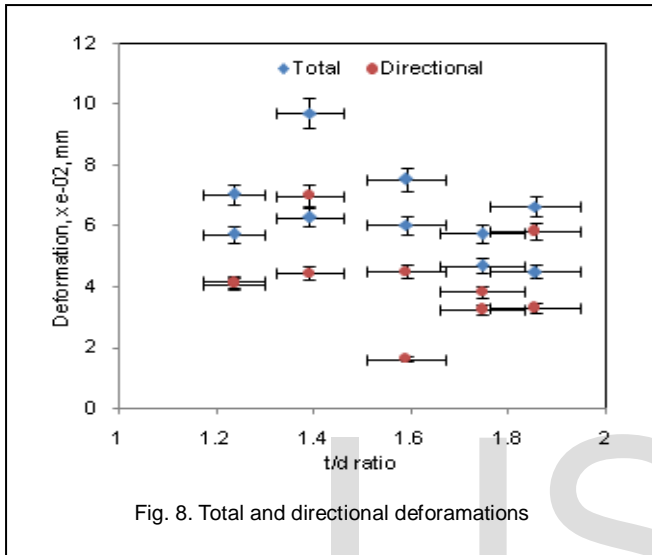


Fig. 8. Total and directional deformations

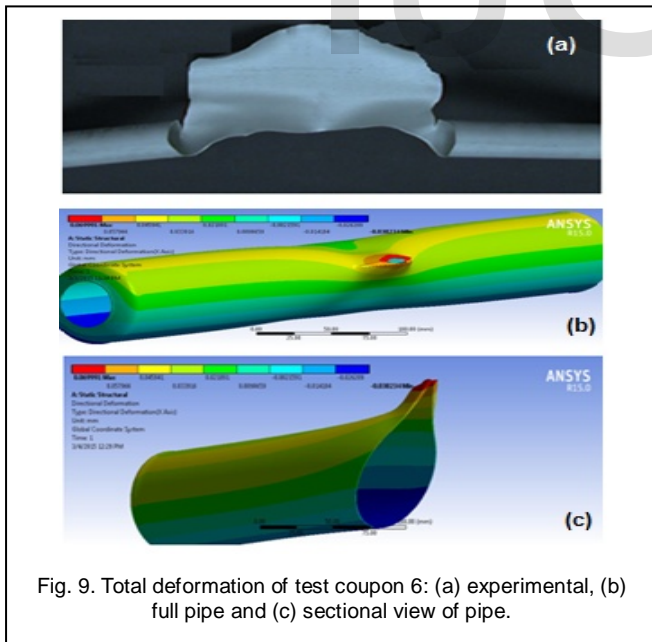


Fig. 9. Total deformation of test coupon 6: (a) experimental, (b) full pipe and (c) sectional view of pipe.

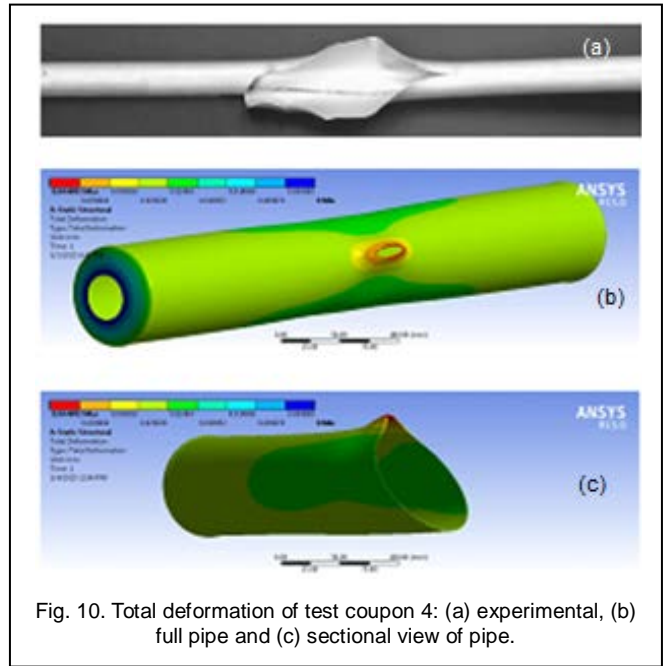


Fig. 10. Total deformation of test coupon 4: (a) experimental, (b) full pipe and (c) sectional view of pipe.

4.2 Stress Distribution across the Crack

The equivalent stress distribution across the crack for all the test coupons subjected to the pressure of 6.1 MPa is shown in figure 11. The maximum equivalent stress was found to be 851.62 MPa for the test coupon 6.

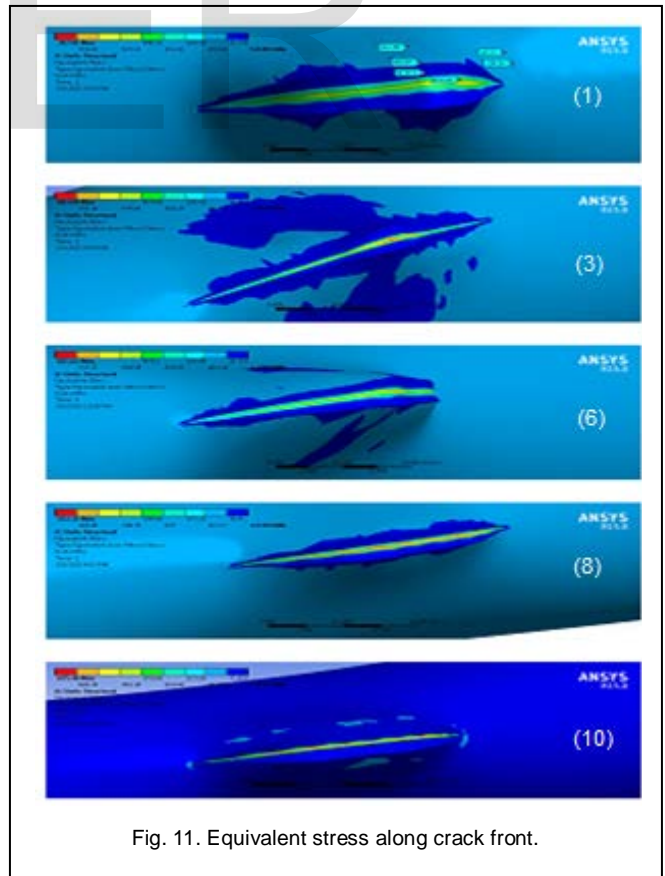


Fig. 11. Equivalent stress along crack front.

Figure 12 presents the shape function for the test coupon calculated by the spiral weight method. The nodal distribution was equally spaced with additional nodes around the crack line and at the crack tip.

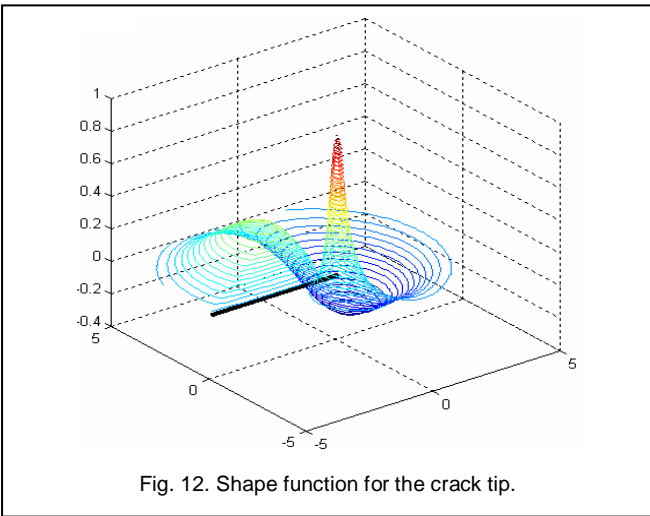


Fig. 12. Shape function for the crack tip.

If the failure is defined by material yielding, it follows that the design goal is to limit the maximum equivalent stress to be less than the yield strength of the material:

$$\frac{\sigma_e}{S_y} < 1 \tag{8}$$

An alternate but less common definition states that fracturing occurs when the maximum equivalent stress reaches or exceeds the ultimate strength of the material:

$$\frac{\sigma_e}{S_u} < 1 \tag{9}$$

The yield strength and tensile strength of 6061 Al alloy are 276 MPa and 310 MPa respectively. The ratio of σ_e/σ_y and σ_e/σ_{ts} are plotted for all the test coupons in figure 13. These were found to be maximum for the test coupons 3 and 6 and to be minimum for the test coupons 4 and 7. This was also observed that both criterion fail with an increase in the bursting pressure.

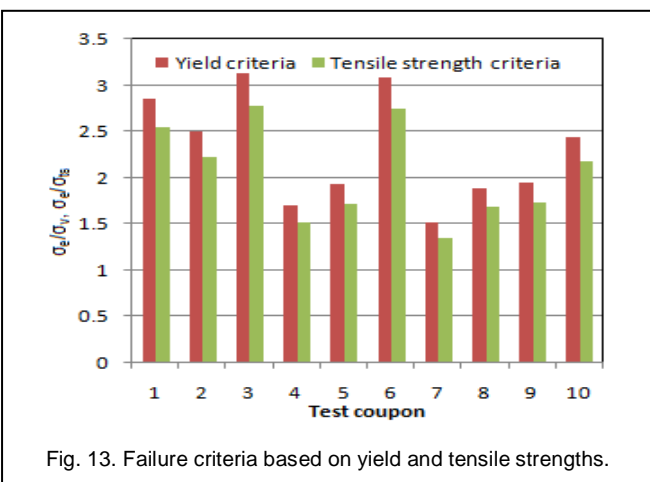


Fig. 13. Failure criteria based on yield and tensile strengths.

4.3 J-Integral

The J-integral is equal to the strain energy release rate for a crack in a body subjected to monotonic loading. The path dependence of the J-integral is displayed for all ten specimens are shown in figure 14. For a crack in an elastic body subject to a load, the elastic energy stored in the body is a function of two independent variables: the displacement of the load, and the area of the crack. The total displacement of the test coupons 4 and 6 were respectively 4.49mm and 9.70 mm. The crack area for the test coupons 4 and 6 were nearly 16.27 mm² and 22.53 mm² respectively. The path dependence of the J-integral was much more significant in a large deformation analysis [14]. The far field value of J was reached with contour # 6 in the latter case, whereas in the small deformation analysis contour # 4 had already reached the far field value.

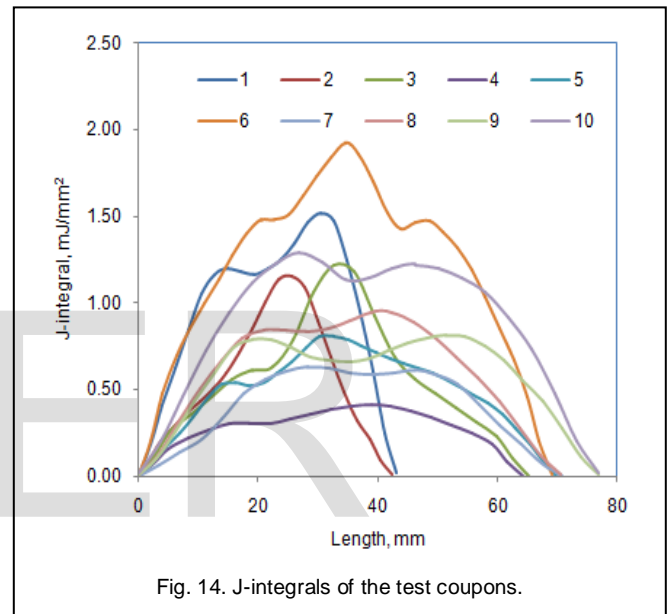


Fig. 14. J-integrals of the test coupons.

4.4 Stress Intensity Factors

Each test coupon was started with a pre-existing crack of a given length "2a". Mode I was a spreading apart of the two halves of the crack interface, recognizable as the most severe case. The stress intensity factor (K) is a defined as the product applied macroscale stress (σ), the square root of the crack length(a), and a constant that depends on the particular fracture mode and geometry of the test specimen. The stress intensity factor for Mode I is designated KI, KII for Mode II, and KIII for Mode III.

Figure 15 shows the variations of stress intensity factors (KI, KII, and KIII) along the initial crack-front. Figures 15(b) and 15(c) indicate that the values of KII and KIII stress intensity factors along the crack-front were very small and, therefore, mode-I was the dominant fracture mode. KIII was much smaller than KII also. Figure 15(a) shows that the mode-I stress intensity factors at the crack-front of all the pipes. The pipe 6 and 4 were reported to have the maximum and minimum values of KI respectively. All stress intensity factors were increased with enlarging the crack length.

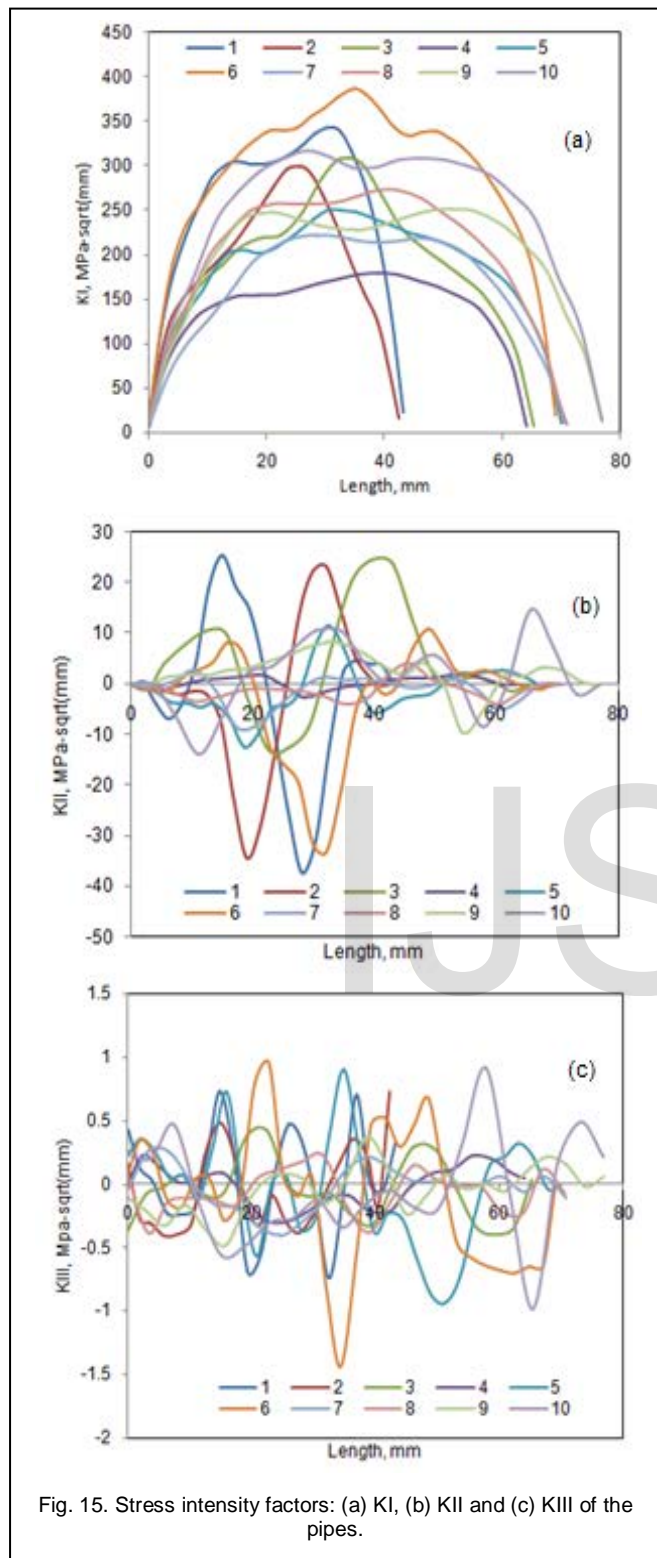


Fig. 15. Stress intensity factors: (a) KI, (b) KII and (c) KIII of the pipes.

5 CONCLUSIONS

In this paper 3D finite element analyses considering a general mixed-mode fracture condition were performed to obtain the crack growth behavior of 6061 Al-alloy pipes subjected to internal bursting pressure. It was observed that the path dependence of the J-integral is much more significant in a large

deformation analysis. The values of KII and KIII stress intensity factors along the crack-front were very small and, the mode-I was the dominant fracture mode.

ACKNOWLEDGEMENTS

The authors thank the University Grants Commission (UGC) - New Delhi for assisting financially this project under PG project assistantship from SAP-UGC project sanctioned to the Department of Mechanical Engineering, JNT University Hyderabad.

REFERENCES

- [1] P. Hopkins, "Training Engineers in Pipeline Integrity," Western Regional Gas Conference, Arizona, EUA, pp.1-9, 2002.
- [2] G. R. K. Kanters, "Pipeline Corrosion and Cracking and the Associated Calibration Considerations for Same Side Sizing Applications," Eclipse Scientific Products Inc., Williamsford, Ontario, Canada.
- [3] BS7910, Guide on Methods for Assessing the Acceptability of Flaws in Metallic Structures- Annex G: The Assessment of Corrosion in Pipes and Pressure Vessels, British Standard, 1999.
- [4] DNV, Recommended Practice DNV RP-F101 Corroded Pipelines, Det Norske Veritas, Norway, 1999.
- [5] G.R.Irwin, "Analysis of stresses and strains near the end of a crack traversing a plate," Applied Mechanics, vol.24, pp.361-364, 1957.
- [6] A. Cosham, P. Hopkins, "Best Practice for the Assessment of Defects in Pipelines-Corrosion", Engineering Failure Analysis, 2007, 1245-1265.
- [7] ANSYS, Inc., www.ansys.com, July 2010.
- [8] D. R. Stephens, B. N. Leis, and D. L. Rudland, "Influence of Mechanical Properties and Irregular Geometry on Pipeline Corrosion Defect Behavior", 1997.
- [9] Chennakesava R Alavala, "CAD/CAM: Concepts and Applications," PHI Learning Pvt. Ltd., 2008.
- [10] Chennakesava R Alavala, "FEM: Basic Concepts and Applications," PHI Learning Pvt. Ltd., 2008.
- [11] N. Jyothirmayi, A. Chennakesava Reddy, B. Balu Naik, "Finite element analysis of Ti-alloy fracture behavior and experimental validation," National Conference on Advances in Mechanical Engineering, Hyderabad, pp.50-55, 13-14th May, 2005.
- [12] A. Chennakesava Reddy, "Finite element analysis of reverse superplastic blow forming of Ti-Al-4V alloy for optimized control of thickness variation using ABAQUS," Journal of Manufacturing Engineering, vol.1, no.1, pp.6-9, 2006.
- [13] Jr. J.Newman, and I. S. Raju, "An Empirical Stress-Intensity Factor Equation for the Surface Crack," Engineering Fracture Mechanics vol.15, no.1-2, pp.185-192, 1981.
- [14] A. Chennakesava Reddy, P. Ram Reddy, B. Kotiveerachari, "Large rotation and large deformation analysis of four-bar mechanism," National Level Technical Symposium Nalgonda, 12th March 2005.